

Off-the-energy-shell effect in the dissociative recombination of HD^+

H. Takagi*

Center for Natural Science, Kitasato University, 1-15-1 Kitasato, Sagami-hara, Kanagawa, 228-8555, Japan

S. Hara

*Tsukuba University of Technology, 4-12-7 Kasuga, Tsukuba-shi, Ibaraki, 305-8521, Japan*H. Sato[†]*Faculty of Science, Ochanomizu University, 2-1-1 Ootuka, Bunkyo, Tokyo, 112-8610, Japan*

(Received 25 November 2007; revised manuscript received 11 December 2008; published 28 January 2009)

The Lippmann-Schwinger (LS) equation for the K matrix is numerically solved for the collision of $\text{HD}^+ + e$ interacting by the configuration interaction (CI). The realistic CI strength is deduced from *ab initio* calculation of electron scattering. The LS equation is extended to the negative collision energies in the context of multichannel quantum defect theory (MQDT) for the dissociative recombination (DR). A decoupling property is shown for the LS equation, which is useful for reducing the amount of the calculation. The Chebyshev quadrature is employed for the calculation and a fully converged result has been obtained. Using the result with the MQDT, the DR cross section of HD^+ is obtained. It has turned out that the off-the-energy-shell contribution is indispensable for understanding the DR. The contribution from the negative energies largely affects the low-energy DR. The DR at low energy is induced by the indirect process with rotational excitation. The separable approximation on the CI is examined for the realistic CI strength. This approximation has turned out to be inadequate for the DR of HD^+ . The calculated rate coefficient reproduces the experiment [A. Al-Khalili *et al.*, *J. Phys. A* **68**, 042702 (2003)] both on the absolute magnitude and resonance structure. The off-the-energy shell contribution largely affects on the initial vibrational state (v^+) dependence. This contribution increases the rate coefficient for $v^+=0$ and decreases for $v^+=2$.

DOI: [10.1103/PhysRevA.79.012715](https://doi.org/10.1103/PhysRevA.79.012715)

PACS number(s): 34.80.Lx, 34.80.Ht

I. INTRODUCTION

The major mechanism of dissociative recombination (DR) of H_2^+ is considered as the incident electrons are captured into the two-electron excited resonance state of which potential curve is dissociative [1,2]. This mechanism, known as the direct process, is induced by the configuration interaction (CI) between the one- and two-electron excited states. Another mechanism named the indirect process is the DR where the incident electron is temporarily recombined into the rotational and/or vibrational excited Rydberg states [3]. These recombined Rydberg states finally dissociate into the two-electron excited state. The CI does not induce the indirect process within the first-order perturbation but the higher-order effect enables it. The nonadiabatic interaction (NAI) is thought to be the main mechanism of the indirect process. The NAI in the Rydberg and electronic continuum states is known to be well represented by the multichannel quantum defect theory (MQDT) [4]. The so-called two-step method [5] enabled us to take account of both the CI and the NAI uniformly. In the first step of this method, a scattering problem of electrons by the CI needs to be solved accurately. Next, the problem of NAI is solved by the MQDT using the electronic state obtained by the first step.

An electronic resonance state plays an important role in the dissociative processes, not only for the DR but also the

dissociative attachment (DA) [6–9]. These dissociative processes are controlled by the nonlocal potential in the space coordinate representation. The nonlocality originates in the energy dependence of CI. If we neglect this dependence and assume the completeness of the vibrational wave functions, the interaction potential becomes local [3]. Thus, the nonlocal treatment means to take into account the CI strength at off-resonance energies. Besides the approach using a space coordinate, it has been studied to solve a spectrum resolved Lippmann-Schwinger (LS) equation which the K matrix satisfies [5,10]. The K -matrix K of real number is easy to calculate compared with other complex collision matrices and it is directly related to the quantum defect, which is the invariant quantity of the MQDT. The LS equation is formally represented by the matrix form as $K = -\pi V + V G_0 K$, where V is the CI, and G_0 is the Green's function of the free stationary state. When we represent this equation by energy resolved form as will be seen in Sec. II A, the term of $V G_0 K$ denotes the contribution from the off-the-energy-shell of the matrix. This off-the-energy-shell term represents higher-order effect of perturbation theory, which is called the Born series. The first-order approximation for the LS equation $K = -\pi V$ has been widely adopted in many studies [11–13]. For more accurate calculation, the second-order approximation $K = -\pi V + V G_0 V$ has been employed, although the K -matrix elements between the dissociative states are neglected [14,15]. A consistent higher-order treatment inevitably requires to investigate energy dependence of the CI strength.

The problem of nonlocality has been studied for the DA by using model interactions [6]. The energy dependence assumed in that model was taken to be given by the threshold

*takagi@kitasato-u.ac.jp

[†]yfa71886@nifty.com

law given by Wigner [16]. This threshold law is actually given for a potential scattering (not for a resonance scattering) and it is valid only for the on-the-energy-shell interaction. The energy dependence of the CI which we need now is off-the-energy-shell matrix elements, that is the CI strength at off-resonance energies. In this paper, we will study the DR using the CI strength obtained by an *ab initio* calculation, which has nonseparable dependence on the electronic energy and the internuclear distance. An essential difference of DR from the DA is the existence of the Rydberg states, which means the off-the-energy-shell contribution from the negative energy of the incident electron. Special care will be paid for this contribution in the present paper.

Several papers have already been presented on the DR of HD⁺ based on realistic CI [10,17–20], where the adopted CI strength was not definitely shown. In the present paper, we show the definite condition of the previous papers for the comparison with the present study based on more detailed investigation on the CI. In the older studies [10,17,18], the quadrature in the LS equation was done by Simpson method, which is not fully converged [21]. We will check the accuracy on the result by the old quadrature.

On the HD⁺ molecule, the DR cross section has been measured specifying the initial vibrational state to be the ground state. The recent measurements using the electron cooler ring have achieved high-energy resolution up to 1 meV and have given precise absolute cross section [22–24]. Several experiments specifying the rotational state are undergoing now. By comparing those experiments with the rigorous calculation, we shall make clear the validity of our theory and the reliability of the storage ring ultracold experiment.

II. ELECTRON-MOLECULE SCATTERING BY CONFIGURATION INTERACTION

A brief report of this section is seen in the progress report by one of the authors (HT) [19,20]. We here show the complete form of the formulation, which is the basis of the present study.

A. Lippmann-Schwinger equation

We adopt the basis functions made up by Born-Oppenheimer (BO) approximation in order to represent a system interacting by the CI. The CI considered now is the interaction between a two-electron excited state labeled by suffix d and one-electron excited one, which is specified by the energy of excited electron ϵ . Setting the coordinates of electrons r collectively, we present the wave functions of those states by $\phi_d(r)$ and $\phi_\epsilon(r)$. The radial nuclear wave functions associated with those electronic functions are, respectively, represented by $F_\epsilon^J(R)$ and $\chi_v^N(R)$. The former is the dissociative wave function of the dissociating energy ϵ and the total angular momentum J . The latter is the wave function of vibrational state v with rotational state N . The internuclear distance is presented by R . The strength of the CI is represented by the following matrix elements of the electronic Hamiltonian of fixed nuclei at R ; $H^{\text{ele}}(r;R)$:

$$V_{v\epsilon,d\epsilon}^{NJ} = \langle \chi_v^N(R) | V_{\epsilon,d}(R) | F_\epsilon^J(R) \rangle_R, \quad (1)$$

where

$$V_{\epsilon,d}(R) = \langle \phi_\epsilon(r;R) | H^{\text{ele}}(r;R) | \phi_d(r;R) \rangle_r. \quad (2)$$

Since the molecular orientation is fixed during the electron collision for the inner region of the MQDT, we assume the rotational transition is frozen for the CI, $N=J$. The rotational transition is taken into account at the second stage of the two-step method separated from the first stage [25]. Thus, we omit the fixed parameter N and J in this section. The total energy is a sum of the energies of electronic and nuclear motion; $E^T = E_v + \epsilon = E_d(R=\infty) + \epsilon$. When we write the total energy as E_ϵ^T for the channel v , and E_d^T for the channel d , the off-the-energy-shell element of the CI strength is represented by

$$V_{v\epsilon,d\epsilon} = V_{v,d}(E_\epsilon^T, E_d^T), \quad (3)$$

where $E_\epsilon^T \neq E_d^T$ in general.

We use Greek characters, for example α , for identifying the channel and E_α for the total energy of the channel α : $\{\alpha\} = \{v\} \cup \{d\}$, $\{E_\alpha\} = \{E_\epsilon^T\} \cup \{E_d^T\}$, where $\{\cdot\}$ shows a set of states and \cup presents the direct sum of the set. The energy resolved LS equation for the K matrix becomes

$$K_{\beta\alpha}(E_\beta, E_\alpha) = -\pi V_{\beta,\alpha}(E_\beta, E_\alpha) + \sum_\gamma \wp_\gamma \int_{-\infty}^{\infty} dE_\gamma \frac{V_{\beta\gamma}(E_\beta, E_\gamma)}{E_\alpha - E_\gamma} K_{\gamma\alpha}(E_\gamma, E_\alpha). \quad (4)$$

The above equation is the same form as Eq. (7.62) given by Newton [26] except for the integral region being extended to the negative energy region. In the MQDT formalism, the CI is represented at the inner region, where the boundary condition on the energy is not imposed. As for the Coulombic basis functions in the inner region of the MQDT, the scattering channel functions should be free from the control of the asymptotic energy boundary condition. The Rydberg states are treated as open channels for the CI interaction.

We can solve this equation by replacing the principal value integral of E_γ to appropriate numerical integration. While the energy is discretized to finite representative points, we use the same notation E_γ (and also E_α and E_β) for the discretized variables as for the continuous one. The algebraic equation to be solved is,

$$\sum_\gamma \sum_{E_\gamma} \left(\frac{V_{\beta\gamma}(E_\beta, E_\gamma)}{E_\alpha - E_\gamma} \omega_{E_\gamma} - \delta_{\beta,\gamma} \delta_{E_\beta, E_\gamma} \right) K_{\gamma\alpha}(E_\gamma, E_\beta) = \pi V_{\beta,\alpha}(E_\beta, E_\alpha), \quad (5)$$

where ω_{E_γ} is weight function of numerical integration and δ is Kronecker delta.

B. Decoupling property

In the present problem, the coupling vanishes between the states of the same electronic configuration; between the d channels or v channels. Due to this character, Eq. (5) could

be separated into two groups. We represent both α and E_α together by italic letter i : $\{i\}=\{\alpha\}\otimes\{E_\alpha\}$, of which states are produced by a direct product of two state functions. Setting the first term in the parentheses of Eq. (5) to A_{ij} , K to x_j , and the right-hand side to B_i , we obtain the following equation. For $\alpha \in \{d\}$, Eq. (5) becomes

$$-x_i + \sum_{j \in \{v\}} A_{ij} x_j = 0, \quad i \in \{d\}, \quad (6)$$

$$\sum_{j \in \{d\}} A_{ij} x_j - x_i = B_i, \quad i \in \{v\}. \quad (7)$$

Equation (7) is rewritten using Eq. (6),

$$\sum_{j \in \{d\}} A_{ij} \sum_{k \in \{v\}} A_{jk} x_k - x_i = B_i, \quad i \in \{v\}. \quad (8)$$

By similar way, we obtain equations for $\alpha \in \{v\}$,

$$-x_i + \sum_{j \in \{d\}} A_{ij} x_j = 0, \quad i \in \{v\}, \quad (9)$$

$$\sum_{j \in \{v\}} A_{ij} \sum_{k \in \{d\}} A_{jk} x_k - x_i = B_i, \quad i \in \{d\}. \quad (10)$$

In Eqs. (8) and (10), the coupling is limited in the subspace of $\{v\}$ or $\{d\}$, respectively. Moreover, Eqs. (6) and (9) are simple linear mapping from the solved complementary subspace.

The number of d channel is usually quite small compared with that of v channel; in the present case, $\{d\}$ consists of one channel and $\{v\}$ consists of 18 channels. This means the amount of calculation could be reduced below one-tenth if we use Eqs. (6)–(10) instead of Eq. (5).

C. Chebyshev quadrature

We have several choices for the quadrature for the first term in the parentheses of Eq. (5). In order to remove the singularity of energy resolvent, the function $V_{\beta\gamma}(E_\beta, E_\gamma) K_{\gamma\alpha}(E_\gamma, E_\alpha)$ should be expanded by known functions, and the integration on E_γ must be done analytically. Pichl and Horáčěk showed that the Chebyshev polynomial is suitable for the basis function for a single channel case [27]. This method is superior in the speed of convergence. Moreover, the analytical integration is simply given by using the Chebyshev polynomials of the first and second kinds.

We here adopt their method to the multichannel energy resolved LS equation (4) after modifying the energy variable transformation [19]. For taking into account the contribution from $\epsilon \leq 0$, that is, the contribution of Rydberg states, we adopted the following transformation from the energy $E_\gamma[a, \infty)$ to $y[1, -1)$:

$$E = \frac{2C}{1+y} + a - C, \quad (11)$$

or

$$y = \frac{2C}{E - a + C} - 1, \quad (12)$$

where a (≤ 0) and C are arbitrary parameters. The parameter a means the lowest energy of the integration and C controls the domain of integration. After this transformation, the term of principal value integration in Eq. (4) is rewritten as the following:

$$\begin{aligned} & \oint_v \int_{-\infty}^{\infty} dE_\gamma \frac{V_{\beta\gamma}(E_\beta, E_\gamma) K_{\beta\gamma}(E_\beta, E_\gamma)}{E_\alpha - E_\gamma} \\ &= \oint_v \int_1^{-1} dy_\gamma \frac{1}{y_\alpha - y_\gamma} \frac{1 + y_\alpha}{1 + y_\gamma} V_{\beta\gamma}(E_\beta, E_\gamma) K_{\beta\gamma}(E_\beta, E_\gamma). \end{aligned} \quad (13)$$

Following Pichl and Horáčěk [27], we expand a part of the right-hand side of the above equation by using the Chebyshev polynomial T_n ,

$$\begin{aligned} & \sqrt{1 - y_\gamma^2} \frac{1 + y_\alpha}{1 + y_\gamma} V_{\beta\gamma}(E_\beta, E_\gamma) K_{\beta\gamma}(E_\beta, E_\gamma) \\ & \sim \sum_{n=1}^N a_n(y_\beta, y_\alpha; \beta, \gamma, \alpha) T_n(y_\gamma). \end{aligned} \quad (14)$$

Adopting this expansion, we can analytically integrate Eq. (13) using the following relation:

$$\begin{aligned} & \int_1^{-1} dy_\gamma \frac{T_n(y_\gamma)}{\sqrt{1 - y_\gamma^2} (y_\alpha - y_\gamma)} = \pi U_{n-1}(y_\alpha), \quad n \geq 1, \\ & = 0, \quad n = 0, \end{aligned} \quad (15)$$

where U_n is the n th-order Chebyshev polynomial of the second kind.

The right-hand side of Eq. (13) becomes

$$\sum_{n=1}^N a_n(y_\beta, y_\alpha; \beta, \gamma, \alpha) \pi U_{n-1}(y_\alpha). \quad (16)$$

The expansion coefficient $a_n(y_\beta, y_\alpha; \beta, \gamma, \alpha)$ is obtained by using the orthogonality of T_n for Eq. (14),

$$\begin{aligned} & a_n(y_\beta, y_\alpha; \beta, \gamma, \alpha) \\ &= \frac{2}{\pi} \int_{-1}^1 dy_\gamma \frac{1 + y_\alpha}{1 + y_\gamma} V_{\beta\gamma}(E_\beta, E_\gamma) K_{\beta\gamma}(E_\beta, E_\gamma) T_n(y_\gamma). \end{aligned} \quad (17)$$

Applying the Gauss-Chebyshev quadrature to the above equation, we obtain the following equation:

$$\begin{aligned} & a_n(y_\beta, y_\alpha; \beta, \gamma, \alpha) \sim \frac{2}{\pi} \sum_{i=1}^M \omega_i (1 + y_\alpha) \\ & \times \sqrt{\frac{1 - y_{\gamma_i}}{1 + y_{\gamma_i}}} V_{\beta\gamma}(E_\beta, E_{\gamma_i}) K_{\beta\gamma}(E_\beta, E_{\gamma_i}) T_n(y_{\gamma_i}), \end{aligned} \quad (18)$$

where $\omega_i = \pi/M$ and $y_{\gamma_i} = \cos[(i-1/2)\omega_i]$. From Eqs. (18), (16), and (4), the LS equation to be solved is

$$\begin{aligned}
K_{\beta\alpha}(E_\beta, E_\alpha) = & -\pi V_{\beta,\alpha}(E_\beta, E_\alpha) \\
& + \sum_{\gamma} \sum_{i=1}^M m(y_\beta, y_{\gamma_i}, y_\alpha; \beta, \gamma, \alpha) K_{\beta\gamma}(E_\beta, E_\gamma)
\end{aligned}
\quad (19)$$

with

$$\begin{aligned}
& m(y_\beta, y_{\gamma_i}, y_\alpha; \beta, \gamma, \alpha) \\
& = \frac{2\pi}{M} (1+y_\alpha) \sqrt{\frac{1-y_{\gamma_i}}{1+y_{\gamma_i}}} V_{\beta\gamma}(E_\beta, E_{\gamma_i}) \sum_{n=1}^N T_n(y_{\gamma_i}) U_{n-1}(y_\alpha).
\end{aligned}
\quad (20)$$

The K matrix is obtained by solving the following algebraic equation which corresponds to Eq. (5):

$$\begin{aligned}
& \sum_{\gamma} \sum_{i=1}^M [m(y_\beta, y_{\gamma_i}, y_\alpha; \beta, \gamma, \alpha) - \delta_{\beta,\gamma} \delta_{E_\beta, E_\gamma}] K_{\gamma\alpha}(E_{\gamma_i}, E_\beta) \\
& = \pi V_{\beta,\alpha}(E_\beta, E_\alpha).
\end{aligned}
\quad (21)$$

III. ELECTRON AND HD⁺ COLLISIONS BY THE CI

A. Adiabatic CI strength

At the collision energies lower than 1 eV, only the lowest two-electron excited state $^1\Sigma_g(2p\sigma_u)^2$ is considered to contribute to the DR if the initial vibrational state of the molecular ion is lower than $v=5$. At the energy of $v=5$, the potential curve of the molecular ion crosses with the second lowest ϕ_d state. We here take into account only the lowest two-electron excited state as the dissociative states ϕ_d . The Rayleigh-Ritz variational method is employed to calculate the two-electron excited state ϕ_d . The ionizing state ϕ_ϵ is calculated in the static exchange approximation with the adiabatic polarization potential. Using those wave functions (ϕ_d, ϕ_ϵ) in Eq. (2), we obtain the CI strength $V_{\epsilon,d}(R)$ [28,29]. The adiabatic resonance width $\Gamma(\epsilon, R)$ is given by

$$\Gamma(\epsilon, R) = 2\pi |V_{\epsilon,d}(R)|^2. \quad (22)$$

These approximations adopted to the electronic states in fixed nuclei are appropriate to present the dynamical processes induced by the CI between the resonance and continuum electronic states. In the scattering theory, the basis functions representing channels are constituted of the eigenfunctions of the total Hamiltonian without the interaction inducing the scattering, which is the CI now. If we adopt the basis functions taking into account the CI, there is no scattering by the CI. The NAI induces all dynamical processes. In such a presentation, we cannot separate the vibrational state from the dissociative state since the electronic states having bonding and dissociative potential curves are mixed. Thus we cannot present the magnitude of the CI as Eq. (1) for an accurate electronic state of which CI matrix elements are diagonal in fixed nuclei. The potential curves of the HD⁺ and the lowest two-electron excited state is shown in Fig. 1. The potential curve by present calculation is higher than the accurate one [12,30], in which the CI is taken into account,

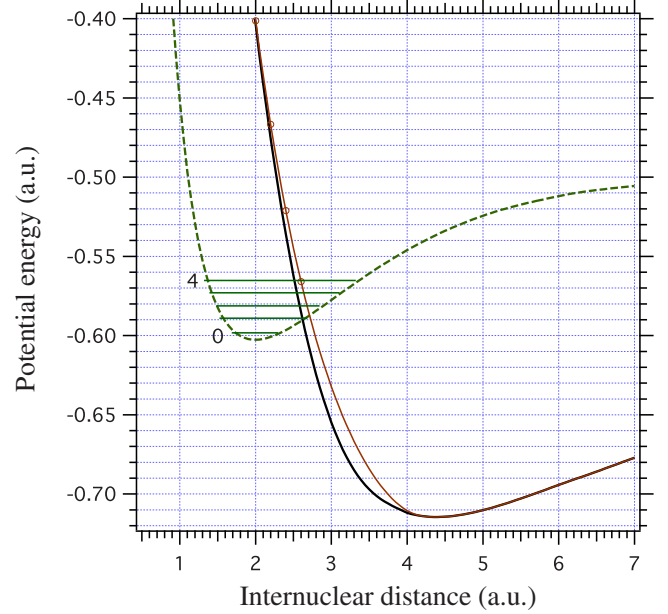


FIG. 1. (Color online) Potential curves of HD⁺ and the lowest two-electron excited state. The higher dissociative curve is given by the present calculation (CI is excluded), and the lower is the more accurate potential curve [12,30] (CI is included). The number shows the vibrational quantum number and the horizontal lines show the energies of vibrational states for HD⁺.

that is, the shift of resonance energy by the CI is included. We intentionally adopted the less accurate potential curve to generate the dissociative nuclear wave function $F_g^J(R)$. The neglected higher-order coupling between the two-electron excited states and continuum states in fixed nuclei is to be recovered by taking account the interaction between them in solving the dynamical process presented by Eq. (21). If we adopted the potential curve where the CI is taken into account, the CI would be counted double.

The crucial important quantity is the strength of interaction $V_{\epsilon,d}(R)$ or $\Gamma(\epsilon, R)$ as a function of two variables ϵ and R . The calculation was done for the internuclear distance $R = 1.0-2.6$ a.u. with the interval of 0.2 a.u., and the collision energy $\epsilon = \sim 0.001-5$ a.u. In Fig. 2, we show the calculated resonance width as a function of the total electronic energy ϵ^T , which is the sum of the collision energy ϵ and the potential energy of hydrogen molecular ion $E_{H_2^+}(R)$, $\epsilon^T = \epsilon + E_{H_2^+}(R)$. As can be seen in Fig. 2, the maximum value of the $\Gamma(\epsilon^T, R)$ comes out at almost fixed total energy ($\epsilon^T \simeq -0.35$ a.u.) for various R . This weak dependence of resonance width on R brings advantage for interpolating or extrapolating the calculated values.

B. Entire picture of adiabatic resonance width

In the present method, the calculation of adiabatic resonance width Γ is confined to positive collision energies but we need it in all energy regions including the negative collision energies. This means we must extrapolate the calculated values to all R and ϵ^T regions. The asymptotic behavior of the Γ is important in the extrapolation. For the negative col-

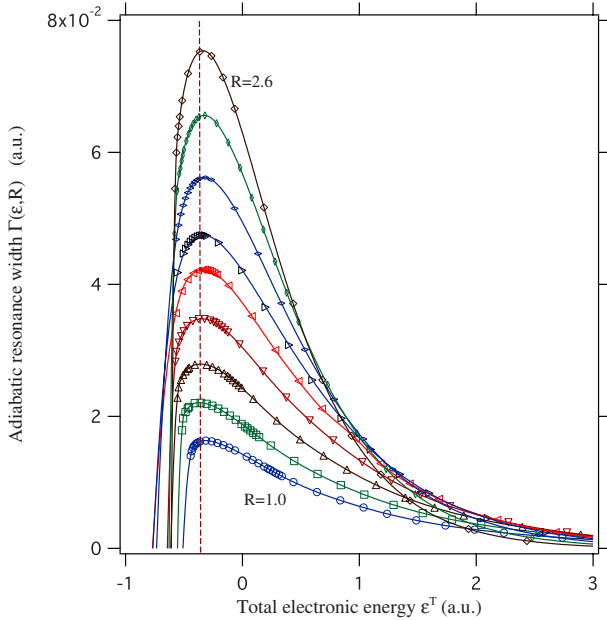


FIG. 2. (Color online) The total electronic energy dependence of the adiabatic resonance width $\Gamma(\epsilon, R)$. The internuclear distance R changes from $R=1.0$ a.u. to 2.6 a.u. with the interval of 0.2 a.u. The curve of larger peak value is the CI strength of larger R . The marks in the figure show the calculated values. The curves show the result of interpolation or extrapolation of the calculated values (see text). The vertical dashed line indicates the total electronic energy $\epsilon^T = -0.35$ a.u.

lision energy ($\epsilon < 0$), the electronic states become discrete Rydberg states, of which energy is represented as $\epsilon = -1/2\nu^2$ with effective quantum number ν . Since there is no state below $\nu \sim 1$, $\Gamma = 0$ for $\epsilon < -1/2$. (i) $\Gamma = 0$ for $\epsilon^T < -1/2 + E_{H_2^+}(R)$, where $E_{H_2^+}(R)$ is the lowest potential energy of the hydrogen molecular ion. The interaction strength sharply becomes zero at the low energy, where collision energy is negative. The Γ decrease quickly when the collision energy becomes negative. The behavior of the Γ in the negative energy sensitively depends on the R as shown in Fig. 2. Thus we carefully fit the calculated values by power series function in the low-energy region and extrapolate them to the negative energy region of $\Gamma = 0$.

When the collision energy becomes large, the continuum wave function frequently oscillates and the overlap between the continuum state and two-electron excited one becomes small. Then the CI strength becomes weak at large ϵ since the CI strength is roughly proportional to that overlap.

(ii) $\Gamma = 0$ for $\epsilon^T \rightarrow \infty$. When the internuclear distance becomes small ($R \rightarrow 0$), the values of $E_{H_2^+}(R)$ become large because of repulsive internuclear force. Then the collision energy becomes negative for a finite ϵ^T . Therefore, (iii) $\Gamma = 0$ for $R \rightarrow 0$. When the R value becomes large, the potential curve of two-electron excited state crosses with the curve of $E_{H_2^+}(R)$, and further large, it merges to a potential curve of Rydberg state, where the CI vanishes. Thus, setting the merging internuclear distance R_m , (iv) $\Gamma = 0$ for $R > R_m$. The potential energy curves of the EF and $(2p\sigma_u)^2$ states indicate $R_m \sim 4.5$ a.u. [31]. The conditions for the asymptotic behav-

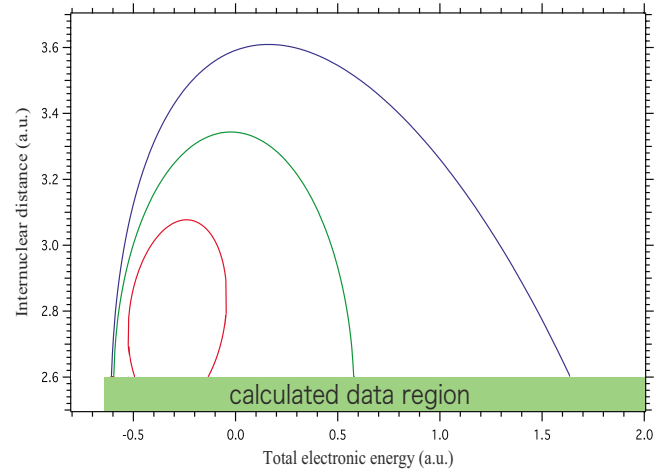


FIG. 3. (Color online) Extrapolation of contour. The three curves show the contours of $\Gamma(\epsilon, R) = 0.07, 0.03, 0.005$ a.u. from the inner to the outer regions.

ior (i)–(iv) confine the Γ in the full region of (ϵ^T, R) space. If we present the Γ in a three-dimensional graph with the Γ on the z axis and the ϵ^T on the x and R on the y axis, the Γ is represented as an isolated island on the sea level, as can be seen in Fig. 4.

We employed the bicubic B -spline interpolation [32] using the calculated (ϵ, R) points. In the outside of the calculated R region ($1.0 \leq R \leq 2.6$ a.u.), we need to extrapolate the calculated values. The B -spline works well for the extrapolation to $R < 1.0$ a.u. because the strength monotonically decreases as R becomes zero.

For the R larger than 2.6 a.u., the extrapolation using the calculated values diverges. Because the Γ forms an isolated island as pointed out before, we extrapolate the contour lines of some Γ values at the boundary of the calculated region ($R = 2.6$ a.u.) assuming that the contour shape could be represented by the quadratic form of ϵ^T and R . Since the contour line necessarily crosses 2 times with that boundary, we introduce a coordinate (x, y) which is the coordinate shifted by the origin of the coordinate (ϵ^T, R) to the crossing point of small ϵ^T . That is $(x, y) = (\epsilon^T - \epsilon_0^T, R - 2.6)$ with ϵ_0^T being the right-hand crossing point with the boundary in Fig. 3. The quadratic form is represented as

$$x^2 + axy + by^2 + cx + dy = 0, \quad (23)$$

using four parameters from a to d . These parameters are determined using two points on the boundary $y = 0$ ($R = 2.6$) in the x - y plane and the gradients of the contour lines (dy/dx) at those two points. We put the position of the larger y crossing point to $(x, y) = (h, 0)$, and the gradient of the contour line there to k_h and the gradient at the smaller y crossing point to k_0 . Then $a = -(k_0 + k_h)/k_0 k_h$, $c = -h$, $d = h/k_0$. One more point on the contour line is needed to determine the values of b , which is less reliable than the extrapolation. We choose three contour lines of $\Gamma = 0.005, 0.03$, and 0.07 a.u., which is shown in Fig. 3. The used parameters are listed in Table I.

TABLE I. Parameters for the quadratic form of the contour.

$\Gamma(\epsilon, R)$	ϵ_0^T	a	b	c	d
0.005	-0.607095	0.722534	0.46	-2.2545	0.73198
0.03	-0.596240	0.03860	0.55	-1.17442	0.0322966
0.07	-0.492700	-0.31029	0.70	-0.35776	-0.200

Adding those values on the contour, we could interpolate and extrapolate the calculated values to the larger R by the two dimensional B -spline method. Figure 4 shows the adiabatic resonance width $\Gamma(\epsilon, R)$ on the whole ϵ^T - R space. The energies of the lowest resonance state $(2p\sigma_u)^2$ at fixed nuclei R is shown by the dashed curve in Fig. 4, which shows the on-the-energy-shell interaction at fixed nuclei. The potential curve of the lowest ionic state is also presented by the dotted curves. The shape of Γ is not simple, especially there is a bump at the low energies of $1.7 < R < 2.4$ a.u., of which effect will be investigated on the low-energy dissociative recombination.

C. Transition probability

The K -matrix elements were calculated by solving Eq. (21). The values of parameters C and a in Eq. (12) were adopted to $C=0.3$ and $a=-0.625$ a.u. (energy of dissociation limit). The number of energy points M in Eq. (21) is adopted to $M=100$ after confirming the obtained K matrix to be converged [20]. The 18 vibrational functions ($v=0-17$) are employed in the calculation. The energy region of the present interest is the incident electron energy lower than 1 eV for $v=0-2$ initial vibrational states, which correspond to the total energies between -0.6 and -0.5 a.u. In order to investigate the effect of the Rydberg states to such low-energy collisions, we calculated the transition probabilities excluding

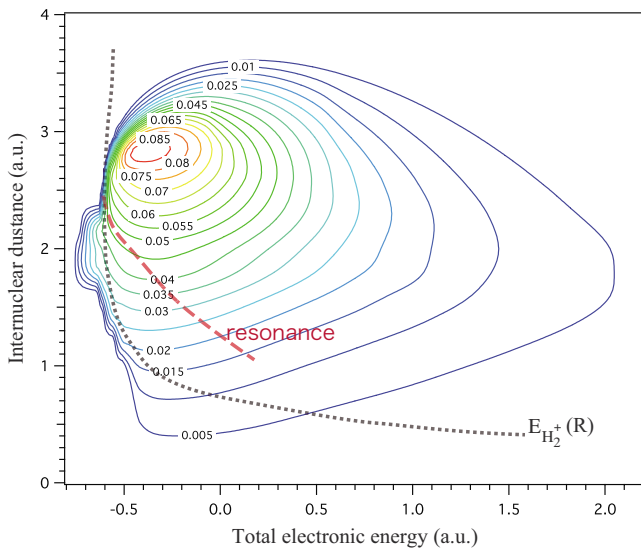


FIG. 4. (Color online) Adiabatic resonance width $\Gamma(R, \epsilon)$ (a.u.). The dashed line indicates the resonance energies of the two-electron excited state $(2p\sigma_u)^2$, the dotted curve indicates the potential curve of hydrogen molecular ion.

the Rydberg states of the principal quantum number lower than n_{cut} . The dissociation probability is defined by square absolute value of the S -matrix element $|S_{d,v}(E)|^2$, where the S -matrix element is deduced from the calculated K matrix, $S=(1+iK)(1-iK)^{-1}$.

Figure 5 shows the calculated dissociation probability from $v=0, 1$, and 2 by changing the value of n_{cut} for the total angular momentum $J=0$. The contribution from the Rydberg states is not negligible at low energies especially for the low initial vibrational state. The results of $n_{\text{cut}}=3$ and 4 are actually the same. Irregular behavior near the zero energies is seen for the Rydberg contribution being limited ($n_{\text{cut}}=50$) in $v=0$ and 1 although the result is almost converged numerically. This irregular behavior can be removed by taking account of the many Rydberg states ($n_{\text{cut}} \leq 6$). If we cut all of the Rydberg states, the magnitudes of $V_{e,d}(R)$ changes discontinuously at $\epsilon=0$. This discontinuity induces a singularity of the calculated K matrix near the zero energy [20] and affects to the dissociation probability.

The calculated dissociation probability was compared with the first-order calculation in Fig. 6. The higher-order effect enhances the probability from the initial vibrational state $v=0$ and reduces that from $v=2$ drastically. As the re-

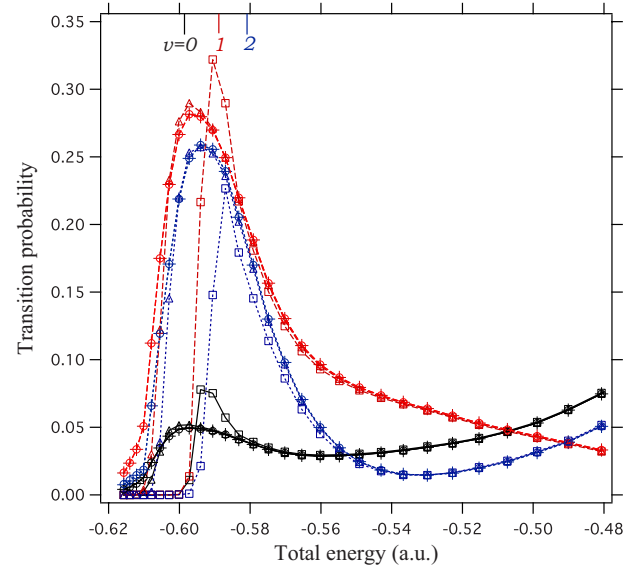


FIG. 5. (Color online) The dissociation probability by the CI for $J=0$; contribution from the Rydberg states ($\epsilon \leq 0$). Solid line indicates the dissociation from $v=0$, dashed line indicates from $v=1$, and dotted line indicates from $v=2$. The marks show the lowest principal quantum number (n_{cut}) of the included Rydberg states: \circ , $n_{\text{cut}}=3$; $+$, $n_{\text{cut}}=4$ (all points coincide with $n_{\text{cut}}=3$); \triangle , $n_{\text{cut}}=6$; \square , $n_{\text{cut}}=50$. The vertical lines indicate the zero collision energies for each initial vibrational state v .

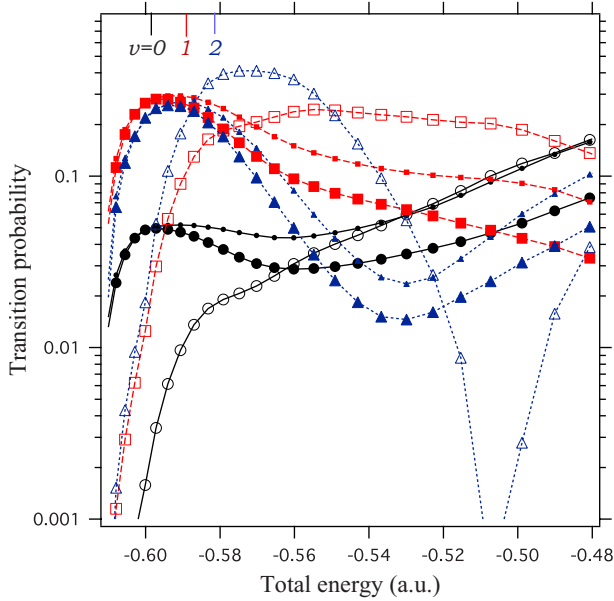


FIG. 6. (Color online) Effect of off-the-energy-shell contribution for $J=0$. The marks and line types indicate the initial vibrational state, line type indicates the same meaning as in Fig. 5; circle, $v=0$; square, $v=1$; triangle, $v=2$. The large filled mark, present result with $v \leq 17$; small filled mark, present result with $v \leq 9$; open mark, first-order calculation with $v \leq 17$.

sult, the magnitudes of those two probabilities become the same order although the first-order calculation gives quite large probability for $v=2$. The $v=2$ initial state is energetically more suitable for the dissociation than the $v=0$ since the energy level of $v=2$ exceeds the energy of the potential curve crossing between the ionic and dissociative states whereas the $v=0$ energy level does not as is seen in Fig. 1. The vibrational excitation by the CI exceeds this advantage of the initial state condition. The difference between the first-order and the higher-order calculation is clear below -0.4 a.u. The off-the-energy-shell contribution has turned out to be crucial for precise description of the dynamics.

The calculation with less vibrational states ($v \leq 9$) is also shown in Fig. 6. Even for lower initial vibrational states, the higher vibrational states are required as the basis functions.

D. Fitting by analytic functions

In order to solve the LS equation, it is preferable to represent the CI strength by analytic functions. In the previous study [10,17–20], the calculated $\Gamma(\epsilon, R)$ was fitted by a function of

$$\Gamma(R, \epsilon) = A(R)[\epsilon - \epsilon_o(R)]^{\nu(R)} \exp[-\alpha(R)(\epsilon - \epsilon_o)], \quad (24)$$

where ϵ_o is the lower energy satisfying $\Gamma(R, \epsilon_o)=0$ and it is represented by the following form:

$$\begin{aligned} \epsilon_o(R) = & -0.05466 - 0.201056 \\ & \times \exp[-10.85897(R - 1.94784)^2]. \end{aligned} \quad (25)$$

We set $\Gamma(\epsilon, R)=0$ below $\epsilon \leq \epsilon_o$. The functions $A(R)$, $\nu(R)$, and $\alpha(R)$ are quadratic polynomials of R as is shown in Table II. These functions are optimal in a sense of least-squares method. The comparison between the calculated result and the fitted one was shown in Fig. 6 of Ref. [10] and a part of those is shown in Fig. 7. It is notable that there are some differences between the calculated and fitted values especially at the low energies in Fig. 7, since we are now interested in the low-energy collisions.

Figure 8 shows the difference in dissociation probability between the previous study (analytic function fitting) [19,20] and the present one (spline fitting). A small set of the vibrational states ($v \leq 9$) are employed to the calculation in this figure. A large difference is seen especially at low energies. The more older result using the Simpson quadrature adopted for Eq. (5) with the analytic function fitting [10,17,18] is also shown in Fig. 8. Although the Simpson quadrature does not give a completely converged result, the difference from the converged Chebyshev quadrature is not as large in the shown low-energy region.

E. Separable approximation

We call it separable approximation if $\Gamma(\epsilon, R)=f(\epsilon)g(R)$. The separable approximation had great advantage if $g(R)$ could be the adiabatic resonance width $\Gamma(\epsilon_{\text{res}}, R)$, where ϵ_{res} is the resonance energy of incident electrons. In this case, the first-order perturbation treatment gives the same result for the separable and nonseparable interactions. The $\Gamma(\epsilon_{\text{res}}, R)$

TABLE II. Fitting parameters for $\Gamma(\epsilon, R)$, where every unit is a.u. Each of A , ν , and α is represented by $a+bR+cR^2$.

Parameter	R	a	b	c
$A(R)$	≤ 1.2	-0.03944975	0.067907	
	1.2–1.8	0.390665	-0.596665	0.254433
	1.8–2.4	-0.17686	0.1674685	0.0053219
	$2.4 \leq$	1.85496	-1.601835	0.389777
$\nu(R)$	≤ 1.68	1.47856	-2.23734	1.00105
	1.68–2.2	-7.09649	7.78586	-1.91822
	$2.2 \leq$	7.9612	-5.95936	1.21852
$\alpha(R)$	≤ 1.835	2.31616	-2.2291	0.968003
	$1.835 \leq$	3.21778	-2.14261	0.654317

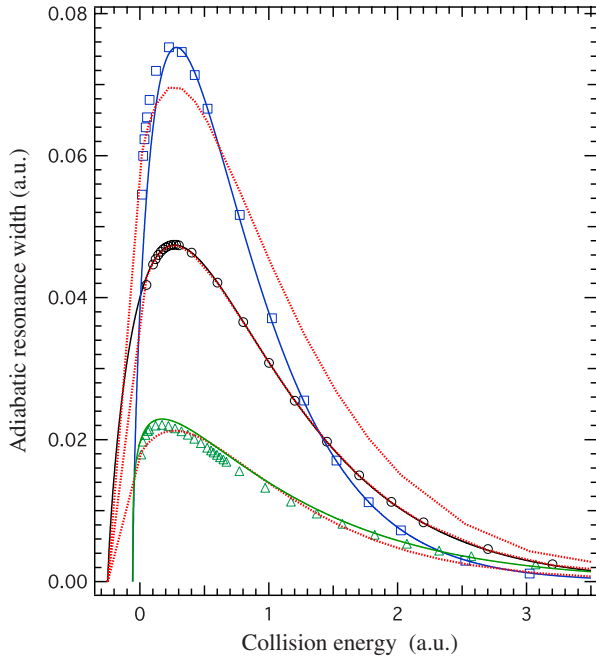


FIG. 7. (Color online) Adiabatic resonance width $\Gamma(\epsilon, R)$: Function fitting and separable approximation. The marks indicate the calculated values at each R : \circ , $R=2.0$ a.u.; \square , $R=2.6$ a.u.; \triangle , $R=1.2$ a.u. The solid curves show nonseparable function fitting, the dotted curves are for separable approximation (see the text).

can be obtained from any electron scattering calculation of fixed nuclei. Unfortunately, the energy dependence of $\Gamma(\epsilon, R)$ around the ϵ_{res} sensitively depends on the R as is shown in Fig. 9. Figure 9 shows the calculated $\Gamma(\epsilon, R)$ as the function of $\epsilon - \epsilon_{\text{res}}$.

Another separable form can be obtained by neglecting the R dependence of the ϵ_0 , ν , and α in Eq. (24). We fixed those parameters at the value of $R=2.0$ a.u., which is the equilibrium internuclear distance of hydrogen molecular ion. They are $\epsilon_0 = -0.249\,863$, $\nu = 0.802\,350$, $\alpha = 1.549\,828$. The function $A(R)$ presenting the R dependence was determined by the least-squares method. The resulting $A(R)$ function became

$$\frac{A(R)}{A(2.0)} = -0.299\,63 + 0.589\,26R + 0.035\,399R^2. \quad (26)$$

Some values of this separable form are also shown in Fig. 7. The difference between the separable and nonseparable form is clear on the graph, especially outstanding for $\epsilon \leq 0$. The value of ϵ_0 at $R=2.0$ a.u. is as small as -0.24 a.u. although it becomes about -0.1 a.u. at $R=1.0$ a.u. or 2.6 a.u.

In Fig. 10, the dissociation probabilities obtained by the separable approximation is compared with those obtained by the function fitting mentioned in the preceding section. The number of adopted vibrational states is 18 ($v \leq 17$). The separable approximation is poor especially at low collision energies. At the zero collision energy, which is indicated by the vertical line in Fig. 10, that approximation underestimates about one-half for $v^+ = 1$ and one-third for $v^+ = 0$. As the collision energy increases, the result by the separable

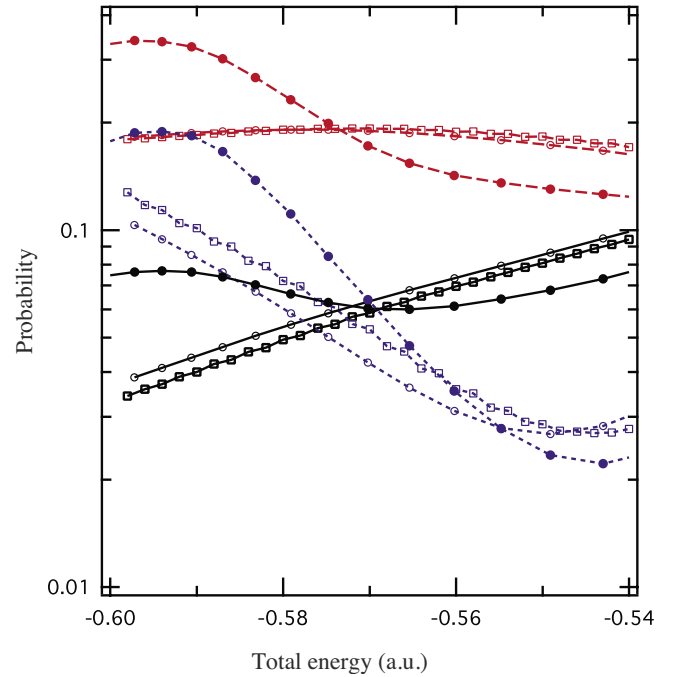


FIG. 8. (Color online) Comparison with previous calculations of dissociation probability for $J=0$. The line types indicate the initial vibrational state as in Fig. 5. The marks indicate method of calculation: \bullet , by Chebyshev quadrature with spline interpolation; \circ , by Chebyshev quadrature with function fitting [19,20]; \blacksquare , by Simpson quadrature with function fitting [10,17,18]. The vibrational states of $v \leq 9$ are used in this figure.

approximation approaches to those by the nonseparable calculation. This means that the contribution from $\epsilon \leq 0$ is important. The poorness of the separable approximation becomes more outstanding if we compare it with the result by spline interpolation. Therefore, the results obtained by the separable approximation [21] is not very accurate.

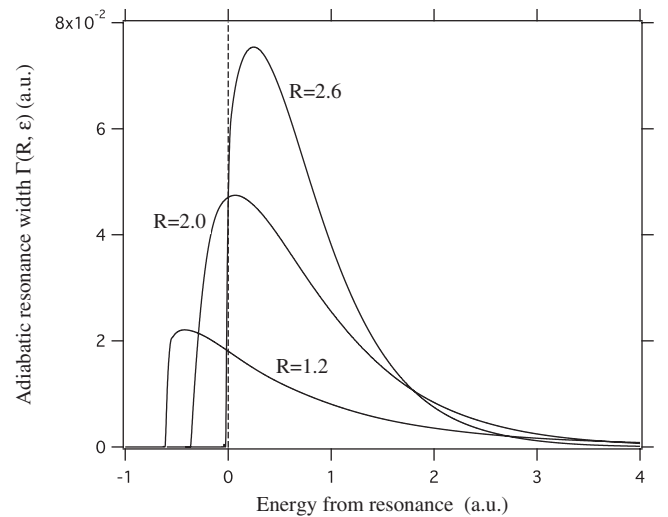


FIG. 9. Adiabatic resonance width $\Gamma(\epsilon, R)$ as the function of $\epsilon - \epsilon_{\text{res}}$ for $R=1.2, 2.0, 2.6$ a.u.

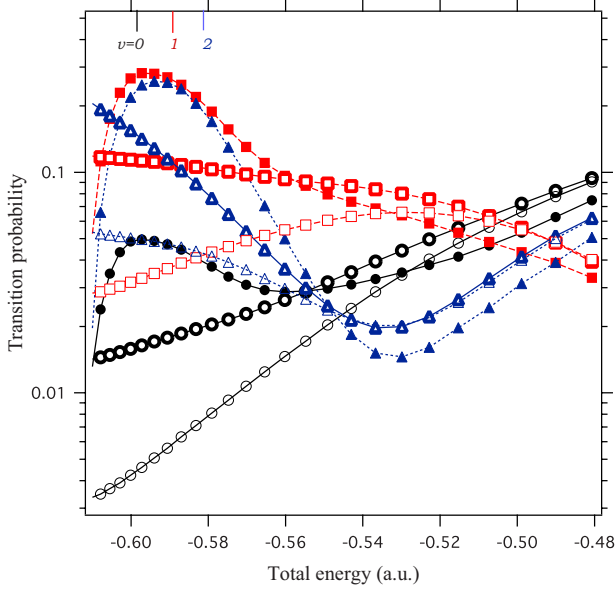


FIG. 10. (Color online) Comparison of dissociation probability by the separable and nonseparable approximations for $J=0$. The shape of mark and line type indicates the initial vibrational state as in Fig. 6. The adopted adiabatic resonance width is indicated by the type of marks: full, spline fitting; bold open, function fitting; thin open, separable approximation of function fitting. The vibrational states included are $v \leq 17$.

IV. DISSOCIATIVE RECOMBINATION

A. MQDT formalism

The calculation of DR cross section by the MQDT was given in the previous studies [13,25]. Schneider *et al.* also presented a formula for the DR [33]. As far as our understanding, their formula is identical to our previous formula although those notations are different. We here summarize some key formulas of the method. First, we diagonalize the K -matrix obtained by the preceding section,

$$\sum_{\alpha', \beta'} U_{\alpha, \alpha'} K_{\alpha', \beta'}(E_\alpha, E_\alpha) U_{\beta', \beta} = -\frac{1}{\pi} \delta_{\alpha, \beta} \tan \eta_\alpha, \quad (27)$$

where U is the unitary matrix diagonalizing the matrix K . The smoothed K -matrix \mathcal{R} defined in MQDT is obtained by the formula

$$\mathcal{R} = \sum_{\Lambda} G^{J\Lambda} (S\mathcal{C}^{-1})^{JN^+\Lambda} G^{J\Lambda}, \quad (28)$$

where

$$G^{J\Lambda}(N^+\ell^+) = \sqrt{\frac{2N^+ + 1}{2J + 1}} C(\ell^+ N^+ J; \Lambda - \Lambda^+, \Lambda), \quad (29)$$

$$G^{J\Lambda}(J_d \Lambda_d) = \delta_{JJ_d} \delta_{\Lambda \Lambda_d}, \quad (30)$$

$$C_{v^+ \ell^+, \alpha}^{JN^+\Lambda} = \sum_{\tilde{\nu} \tilde{\ell}} \langle \chi_{v^+}^{N^+\Lambda^+}(R) | \cos[\pi \mu_{\tilde{\ell} \Lambda}(R) + \eta_\alpha^{J\Lambda}] M_{\ell^+ \tilde{\ell}}(R) \times | \chi_v^{J\Lambda}(R) \rangle U_{v \tilde{\ell}, \alpha}^{J\Lambda}, \quad (31)$$

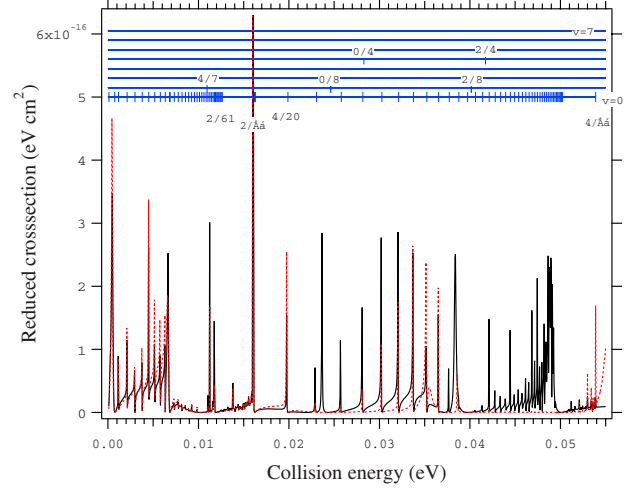


FIG. 11. (Color online) Reduced DR cross section of $\text{HD}^+(v^+=0, N^+=0)$. The adopted adiabatic resonance width is presented by dotted lines, function fitting; solid lines, spline interpolation. The horizontal long lines with cross marks present the energies of rotational (N) and/or vibrational (v) excited Rydberg states, of which principal quantum numbers (n) are less than 58. The lowest horizontal long line is for $v=0$, and the higher one presents the higher v up to $v=7$. The two numbers indicate N/n .

$$C_{d, \alpha}^{JJ_d \Lambda} = \cos(\eta_\alpha^{J\Lambda}) U_{d, \alpha}^{J\Lambda}, \quad (32)$$

and S is obtained by replacing the \cos function to the \sin in the above two equations, where $\mu_{\tilde{\ell} \Lambda}(R)$ denotes adiabatic quantum defect and $\chi_v^{J\Lambda}(R)$ is the vibrational wave function with the total angular momentum (AM) J , electronic AM around the molecular axis Λ , and vibrational state v , and $M_{\ell^+ \tilde{\ell}}(R)$ denotes the mixing matrix of the electronic partial waves ℓ^+ in the eigenchannel $\tilde{\ell}$. The superscript+ means the quantity of ion molecule or incident electron, and suffix d indicates the quantity of the dissociative state. The real K -matrix R , which satisfies the boundary conditions, are given [34] by

$$R = \mathcal{R}_{oo} - \mathcal{R}_{oc}(\mathcal{R}_{cc} + \tan \pi \nu)^{-1} \mathcal{R}_{co}, \quad (33)$$

where the suffix $o(c)$ indicates open (closed) channels, and ν is the effective principal quantum number. The cross section of the DR is obtained using the S -matrix $S = (1 - iR)^{-1}(1 + iR)$ as the following [25]:

$$\sigma_{d, v^+ N^+}^{\text{DR}} = \frac{\pi}{k^2} \rho \sum_J \frac{2J + 1}{2N^+ + 1} \sum_{\ell^+} |S_{Jd, v^+ N^+ \ell^+}^J|^2. \quad (34)$$

Here k is the wave number of the incident electron, ρ is the ratio of the initial multiplicity to the final one.

B. Dissociative recombination of HD^+

The $d\sigma$ partial wave is the most dominant partial wave contributing to the resonance state ϕ_d . We took into account only this $d\sigma$ partial wave as the electronic continuum state ϕ_ϵ in $\text{HD}^+ + e$. We employed the same electronic parameters as the previous calculation [12,30] except for the dissociative

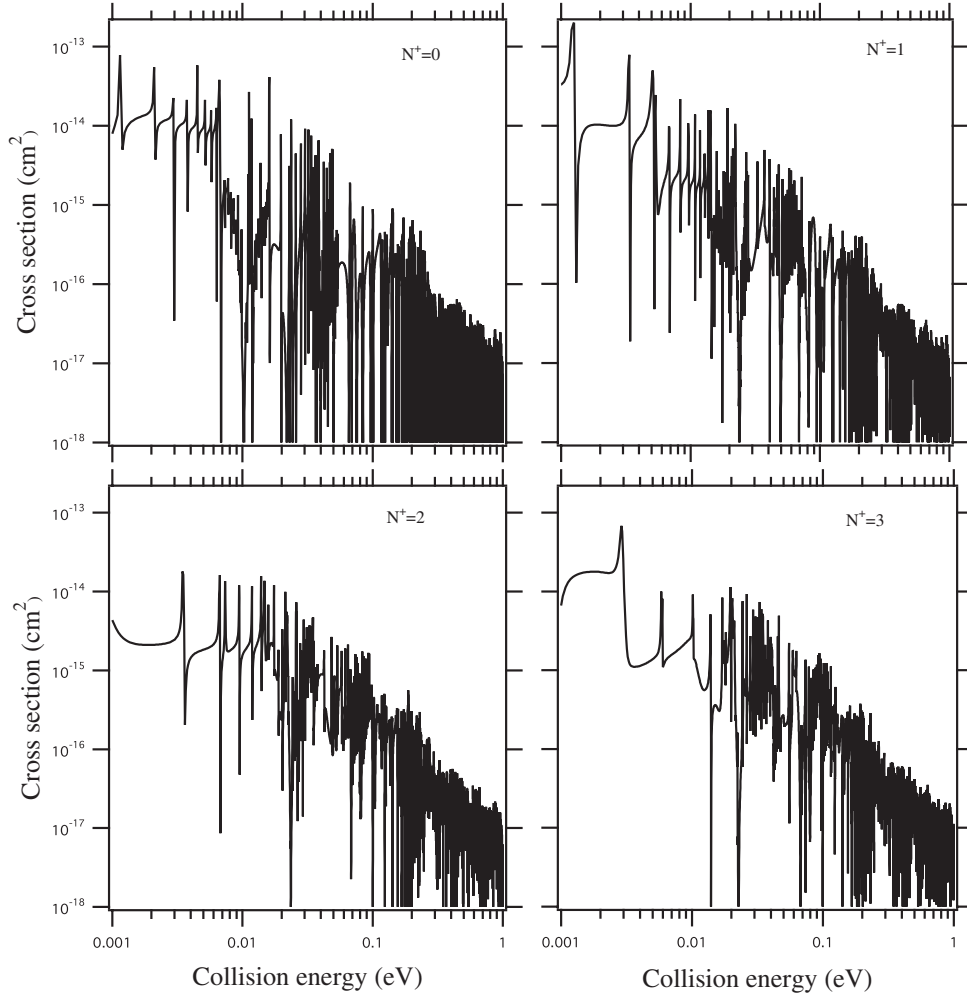


FIG. 12. Dependence of DR cross section for HD^+ on the initial rotational quantum number N^+ for $v^+=0$.

potential curve (see Fig. 1): Ionic potential curve and the adiabatic quantum defect. The contribution from the two-electron excited state was carefully excluded from the adiabatic quantum defect. The minor component $s\sigma$ contributes about 30% at most to the DR [33]. We consider that the contribution of s wave is negligible at low energies because the s wave does not induce the rotational excitation, which will turn out to be the main mechanism of the DR in the following section.

In Fig. 11, we show an example of the present DR cross section of HD^+ of which initial vibrational state (v^+) is $v^+=0$, and the rotational state (N^+) is $N^+=0$. The vertical axis shows the cross section multiplied by the collision energy, which is sometimes called reduced cross section ($\text{cm}^2 \text{eV}$), in order to see the cross section accurately over a wide range of collision energy. The result using function fitting for the adiabatic resonance width is also shown by the dotted line. The energy of rotational and/or vibrational excited Rydberg state is shown by the horizontal long line and cross mark in the upper part of the figure. Almost all peak structures appear at the energies of rotational excited and vibrational unexcited Rydberg states. This indicates the indirect process through the rotational excitation is the dominant mechanism of low-energy DR. The result using the function fitting gave the

same peak positions as the present accurate interpolation, but the magnitudes are different, especially outstanding is the structure seen around 0.045 eV.

We show the rotational dependence of the DR cross section in Fig. 12, where the initial vibrational state is in the ground state ($v^+=0$), and the rotational state (N^+) is $N^+=0-3$. Strong dependence on the initial rotational state is seen at the energy lower than 0.1 eV.

We compare the calculated rate coefficients with experimental results [24,35] for the DR of $\text{HD}^+(v=0)$. The calculated result was convoluted by the energy resolution of 1 meV for transversal to the incident beam direction and 0.05 meV for the longitudinal one. The convoluted rate coefficient Y^{conv} is represented by the convolution of the cross section $\sigma(E)$ with the collision energy E using the convolution function $I(E, E_0)$ [36],

$$Y^{\text{conv}} = \sqrt{\frac{2}{\pi m k T_{\perp}}} \frac{1}{k T_{\parallel}} \sqrt{\frac{1}{k T_{\parallel}}} \int_0^{\infty} dE E \sigma(E) I(E, E_0). \quad (35)$$

The convolution function is given by

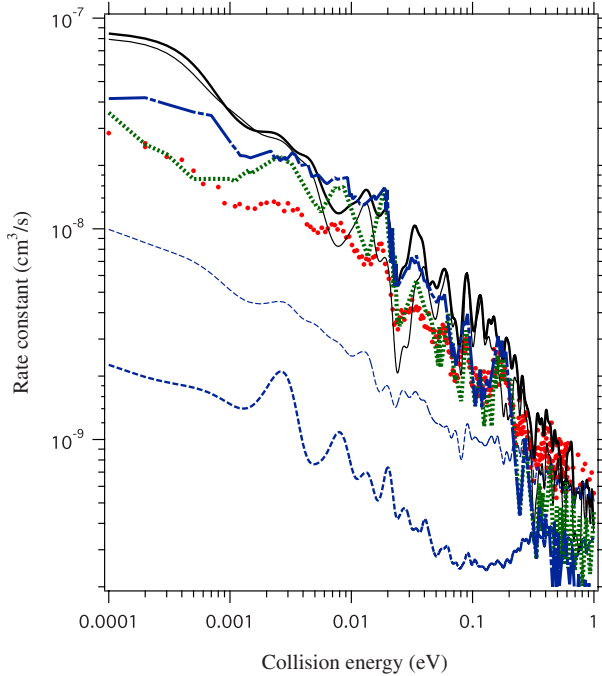


FIG. 13. (Color online) The rate coefficient of DR for HD^+ with $v^+=0$. The experiments shown with dots, TARN II [35]; bold dotted curve, CRYRING [24]; bold dashed-dotted curve, TSR [24]. The calculations are bold solid curve, the present result; thin solid curve, analytic function fitting; bold dashed curve, the first-order approximation without the CI; thin dashed curve, the first-order calculation with the CI (see the text).

$$I(E, E_o) = \frac{1}{2} \sqrt{\frac{\pi k T_{\perp} T_{\parallel}}{E(T_{\perp} - T_{\parallel})}} \exp\left(\frac{E_o}{k(T_{\perp} - T_{\parallel})} - \frac{E}{kT_{\perp}}\right) \times [\text{erf}(\beta) - \text{erf}(\alpha)], \quad (36)$$

where

$$\left(\frac{\alpha}{\beta}\right) = \mp \sqrt{\frac{E}{k} \left(\frac{1}{T_{\parallel}} - \frac{1}{T_{\perp}}\right)} - \sqrt{\frac{E_o}{kT_{\parallel}}} \sqrt{\frac{T_{\perp}}{T_{\perp} - T_{\parallel}}}. \quad (37)$$

The T_{\perp} and T_{\parallel} , respectively, show the fluctuation temperatures of the longitudinal and transverse directions. We also convoluted the rate coefficient on the initial rotational states assuming the thermal distribution of 300 K.

The convoluted rate coefficients are shown in Fig. 13, where these are compared with the experiment by the three storage ring facilities: TARN II [35], CRYRING, TSR [24]. The rate coefficients measured by these three facilities excellently agree with each other on the resonance structure as the peak positions. The magnitude of the rate measured by TSR is, however, about 2 times larger than that by TARN II. The magnitudes tend to be large as the resolution of experiment becomes high [36]. The present calculation represents almost all resonance structure in the experiments except for several peaks at the collision energies of 8 meV and 0.12 eV. More detailed study is required by specifying the initial rotational state. The present calculation represents the experiment by TSR fairly well including the absolute magnitude.

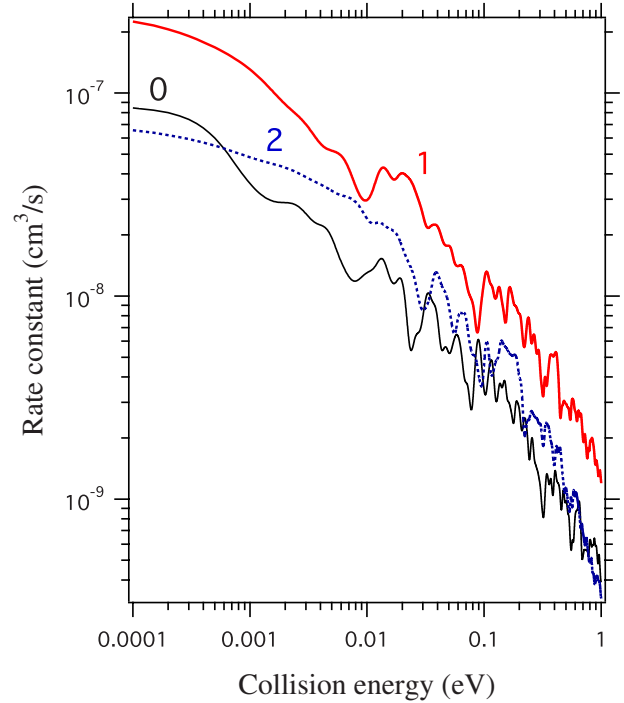


FIG. 14. (Color online) Dependence of DR cross section for HD^+ on the initial vibrational state. The number beside the curve indicates the vibrational quantum number. The electron fluctuation and the rotational state distribution are the same as those of Fig. 13.

We also show three types of calculations other than the present one in Fig. 13. The present calculation consists of the solution of the LS equation (Sec. II) with B -spline fitting (Sec. III B). The other calculations are that with analytic function fitting (Sec. III D), the first-order approximation using the dissociative potential curve neglecting the CI, and that including the CI (see Fig. 1). Large effect of the off-the-energy-shell contribution is clearly seen in the difference between the first-order calculation and the present result. The rate is enhanced over one order of magnitude by the off-the-energy-shell contribution at the collision energies lower than 0.2 eV, which has been already pointed out in the previous calculation [17,18]. By using the dissociative potential curve where the CI is included, the first-order approximation gives a considerably improved result on the magnitude of the rate coefficient. It is, however, not enough to represent the experiments or the present calculation both on the magnitudes and on the structure by the indirect process. The result using the spline fitting for the adiabatic resonance width agrees with the experiments better than that by analytic function fitting. The DR depends on the detail of adiabatic resonance width in the full space of ϵ^T and R .

An important off-the-energy-shell effect can be seen in the dissociation probability given in Fig. 6. The dissociation probability from $v=2$ states is drastically decreased by the off-the-energy-shell effect. On the other hand, this effect enhances the probability of the dissociation from $v=0$ states. These effects on the dissociation probability also appear in the DR rate coefficients. The dependence of DR on v^+ is shown in Fig. 14: The off-the-energy-shell contribution remarkably affects the dependence on the initial vibrational

state in the DR. This vibrational dependence of the DR cross section has been measured by Zajfman *et al.* at the zero collision energy [37,38]. The present calculation and that experiment gave weak dependence on the initial vibrational states whereas the first-order calculations gave sensitive dependence on it.

V. CONCLUDING REMARKS

The off-the-energy-shell contribution to the DR of HD⁺ was investigated based on the realistic electronic states obtained by *ab initio* method. The result by the first-order calculation needs to be corrected at least for the processes related to the lowest two-electron excited state. The DR cross

section depends on the detail of the CI as the function of the energy and internuclear distance. The dissociative processes are largely affected by the off-the-energy-shell contribution of negative energies. The DR at low energy has turned out to be induced by the indirect process with rotational excitation. The DR rate coefficient of the HD⁺ including the off-the-energy-shell contribution nicely represents the resonance structure in the experimental DR rate coefficient.

ACKNOWLEDGMENT

One of the authors (H.T.) would like to thank Professor Tetsumi Tanabe for imparting various information on the DR.

-
- [1] D. R. Bates, *Phys. Rev.* **77**, 718 (1950).
 [2] D. R. Bates, *Phys. Rev.* **78**, 492 (1950).
 [3] J. N. Bardsley, *J. Phys. B* **1**, 349 (1968).
 [4] C. Jungen and O. Atabek, *J. Chem. Phys.* **66**, 5584 (1977).
 [5] A. Giusti, *J. Phys. B* **12**, 3867 (1980).
 [6] M. Berman, C. Mündel, and W. Domcke, *Phys. Rev. A* **31**, 641 (1985).
 [7] C. Mündel, M. Berman, and W. Domcke, *Phys. Rev. A* **32**, 181 (1985).
 [8] J. Horáček and W. Domcke, *Phys. Rev. A* **53**, 2262 (1996).
 [9] M. Čížek, J. Horáček, and W. Domcke, *J. Phys. B* **31**, 2571 (1998).
 [10] H. Takagi, *Dissociative Recombination: Theory, Experiment, and Application II* (Plenum, New York, 1993), p. 75.
 [11] A. Giusti-Suzor, J. N. Bardsley, and C. Derkits, *Phys. Rev. A* **28**, 682 (1983).
 [12] K. Nakashima, H. Takagi, and H. Nakamura, *J. Chem. Phys.* **86**, 726 (1987).
 [13] H. Takagi, N. Kosugi, and M. L. Dourneuf, *J. Phys. B* **24**, 711 (1991).
 [14] S. L. Guberman and A. Giusti-Suzor, *J. Chem. Phys.* **95**, 2602 (1991).
 [15] A. P. Hickman, *J. Phys. B* **20**, 2091 (1987).
 [16] E. P. Wigner, *Phys. Rev.* **73**, 1002 (1948).
 [17] T. Tanabe *et al.*, *Phys. Rev. Lett.* **75**, 1066 (1995).
 [18] H. Takagi, *Dissociative Recombination: Theory, Experiment, and Application III* (World Scientific, Singapore, 1996), p. 174.
 [19] H. Takagi, *Atomic Collision Research in Japan* (Society for Atomic Collision Research, Tokyo, 1998), Vol. 24, p. 3.
 [20] H. Takagi, *Dissociative Recombination: Theory, Experiment, and Application IV* (World Scientific, Singapore, 2000), p. 180.
 [21] L. Pichl, H. Nakamura, and J. Horáček, *Comput. Phys. Commun.* **124**, 1 (2000).
 [22] C. Strömholm *et al.*, *Phys. Rev. A* **52**, R4320 (1995).
 [23] T. Tanabe *et al.*, *Dissociative Recombination: Theory, Experiment, and Application IV* (World Scientific, Singapore, 2000), p. 170.
 [24] A. Al-Khalili *et al.*, *J. Phys. A* **68**, 042702 (2003).
 [25] H. Takagi, *J. Phys. B* **26**, 4815 (1993).
 [26] R. G. Newton, *Scattering Theory of Wave and Particles*, 2nd ed. (Springer-Verlag, New York, 1982).
 [27] L. Pichl and J. Horáček, *J. Phys. A* **29**, L405 (1996).
 [28] S. Hara and H. Sato, *J. Phys. B* **17**, 4307 (1984).
 [29] H. Sato and S. Hara, *J. Phys. B* **19**, 2611 (1986).
 [30] H. Takagi and H. Nakamura, *J. Chem. Phys.* **88**, 4552 (1988).
 [31] L. Wolniewicz and K. Dressler, *J. Mol. Spectrosc.* **67**, 416 (1977).
 [32] W. H. Press, S. A. Teukolsky, W. T. Vetterling, and B. P. Flannery, *Numerical Recipes*, 2nd ed. (Cambridge University Press, Cambridge, 1992).
 [33] I. F. Schneider *et al.*, *J. Phys. B* **30**, 2687 (1997).
 [34] M. J. Seaton, *J. Phys. B* **2**, 5 (1969).
 [35] T. Tanabe *et al.*, *Dissociative Recombination: Theory, Experiment, and Application IV* (World Scientific, Singapore, 2000), p. 170.
 [36] H. Takagi, *J. Phys.: Conf. Ser.* **4**, 155 (2005).
 [37] D. Zajfman, Z. Amitay, C. Broude, P. Forck, B. Seidel, M. Grieser, D. Habs, D. Schwalm, and A. Wolf, *Phys. Rev. Lett.* **75**, 814 (1995).
 [38] D. Zajfman *et al.*, *Dissociative Recombination: Theory, Experiment, and Application IV* (World Scientific, Singapore, 2000), p. 146.